Monolithic Wavelength Converters for High-Speed Packet-Switched Optical Networks

Vikrant Lal, *Member, IEEE*, Milan L. Mašanović, *Member, IEEE*, Joseph A. Summers, *Member, IEEE*, Greg Fish, and Daniel J. Blumenthal, *Fellow, IEEE*

***Abstract*—This paper describes the design and demonstration of advanced 40-Gb/s return-to-zero (RZ) tunable all-optical wavelength converter technologies for use in packet-switched optical networks. The device designs are based on monolithic integration of a delayed interference Mach–Zehnder interferometer (MZI) semiconductor optical amplifier (SOA) wavelength converter with a sampled-grating distributed Bragg reflector tunable laser and an on-chip waveguide delay. Experimental results are presented demonstrating error-free wavelength conversion with 1-dB power penalty at 40-Gb/s data rates. By incorporating label modulation functionality on-chip along with a fast tunable 40-Gb/s wavelength converter, fully monolithic packet-forwarding chips are realized that are capable of simultaneous error-free wavelength conversion of 40-Gb/s payloads, remodulation of 10-Gb/s packet headers, and data routing through fast wavelength switching.**

***Index Terms*—Mach–Zehnder interferometer, photonic integrated circuits, tunable laser, tunable wavelength converter, wavelength conversion, wavelength converter.**

I. Introduction

THE past decade has seen a revolution in the field of information technology. The demand for data communication grew explosively in the mid-1990s and has been steadily increasing since [1]. Recent studies have shown that traffic over the Internet has been increasing at a rate between 70% and 150% per year since 1997 [2] and this trend is expected to continue over the next decade as well. With an ever-increasing demand for bandwidth, one of the possible solutions for the future fiber optic backbone networks is optical packet switching [3]–[5]. Utilizing optical packet switching with wavelength-division-multiplexed (WDM) high data rate channels could solve the issues related to network capacity, utilization, and flexibility. Optical packet switching relies on the ability to individually convert optical data packets between different wavelengths in order to implement the switching functionality in the core of an optical packet switch. The key to making optical packet switching practical and cost-effective is in realizing the full potential of photonic integrated circuits (PICs). New PIC technologies are needed to allow for implementation of routing functions in the optical domain, one of the key features of optical packet switching.

Manuscript received July 20, 2006; revised August 30, 2006. This work was supported by the Defense Advanced Research Projects Agency (DARPA) MTO DOD-N Program under the LASOR Project W911NF-04-9-0001.

V. Lal is with Infinera Corporation, Sunnyvale, CA 94089 USA (e-mail: lal@ece.ucsb.edu).

M. L. Mašanović, J. A. Summers, and D. J. Blumenthal are with the Department of Electrical and Computer Engineering, University of California at Santa Barbara, Santa Barbara, CA 93106 USA (e-mail: mashan@ece.ucsb.edu; jsummers@engineering.ucsb.edu; danb@ece.ucsb.edu).

G. Fish is with JDS Uniphase Corporation, Milpitas, CA 95035 USA (e-mail: g.fish@jdsu.com).

Digital Object Identifier 10.1109/JSTQE.2006.884406

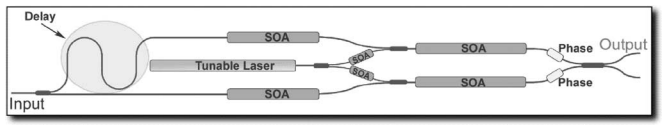

Fig. 1. Schematic diagram of the monolithic widely tunable wavelength converter showing the various functional elements.

The focus of this paper is the design and demonstration of advanced 40-Gb/s return-to-zero (RZ) tunable all-optical wavelength converter technologies for use in packet-switched optical networks. The device designs are based on monolithic integration of a delayed interference Mach–Zehnder interferometer (MZI) semiconductor optical amplifier (SOA) wavelength converter with a sampled-grating distributed Bragg reflector (SGDBR) tunable laser and an on-chip delay. Three device generations are presented: the first generation, realized in an offset quantum-well integration platform; the second generation, utilizing a modified offset quantum-well platform (OQW) with bulk active region MZI-SOAs; and finally, the third generation, called the packet-forwarding chip (PFC), which integrated three major functions required for a high-speed packet-switched network node on a single chip—fast wavelength switching, wavelength conversion, and electro-optic label encoding.

II. Monolithic Tunable SOA-MZI Wavelength Converters—Design and Operation

Fig. 1 shows a schematic of a monolithic widely tunable differential delay MZI-SOA wavelength converter. The device consists of an SGDBR laser, a differential MZI-SOA (DMZI) wavelength converter, an integrated delay arm, and several preamplifier and booster SOAs [6]. The device is 7 mm long and 0.5 mm wide, and requires a single-input and a single-output fiber. The on-chip SGDBR laser is designed to provide continuous tuning over more than 30 nm. The SOA-MZI has 1.2-mm-long SOAs in each branch to achieve the nonlinear phase change. A 10-ps differential delay line is integrated using strongly confined waveguide technology which allows for the small footprint of this component.

A. Differential MZI

High-speed operation of differential SOA-MZI-based wavelength converters is enabled by the fast carrier depletion process, caused by the stimulated recombination induced by the high peak power pump pulse. Due to the high peak powers

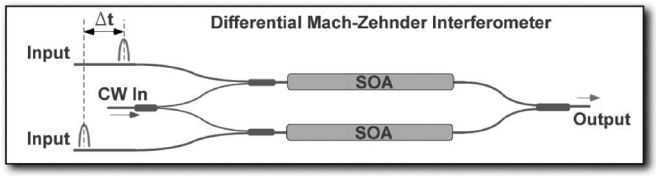

Fig. 2. Schematic of the DMZI scheme.

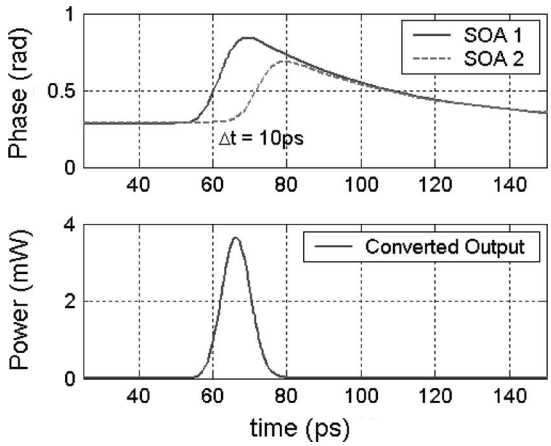

Fig. 3. Simulation of the DMZI scheme. The graphs show the phase modulation in each arm of the MZI (*top*) and the resulting wavelength-converted signal at the output (*bottom*).

associated with the optical pulse, the recombination rate is very high, which leads to a fast carrier depletion. The phase change, that occurs as a result of the carrier depletion, is converted to an amplitude change by using an interferometric structure, in this case, an MZI [7]–[9]. Since the process requires high peak powers, it is best suited for operation with RZ data formats. Time-delayed interference schemes can be used to equalize the slow carrier recovery time, and use only the carrier depletion process to create the switching window. Integrated approaches that have been used in the past to accomplish this are the delayed interference signal converter (DISC) [10] and the DMZI [11].

A schematic explaining the DMZI operation is shown in Fig. 2. The input data signal is coupled into both arms of the MZI with a fixed time delay between the two data streams. The continuous-wave (CW) signal is coupled equally into both MZI arms and is recombined at the output.

The time delay between the two input data streams determines the interferometer switching window. The MZI is set to an OFF state by biasing the two arms to a phase difference of π. A data pulse reaching the top SOA causes carrier depletion, and the resulting cross-phase modulation opens the MZI gate. After a certain time delay, the data pulse in the bottom SOA induces the same phase change on the CW signal in that branch. If the carrier recovery lifetime is much slower than the time delay between the data pulses, the delayed input signal effectively cancels the phase change caused by the upper arm and turns the MZI back off again. This process is illustrated in the simulation shown in Fig. 3. The phase modulation in the second MZI arm brings the phase difference between the two arms back down to zero after a time delay. The amplitude of the phase change in the second

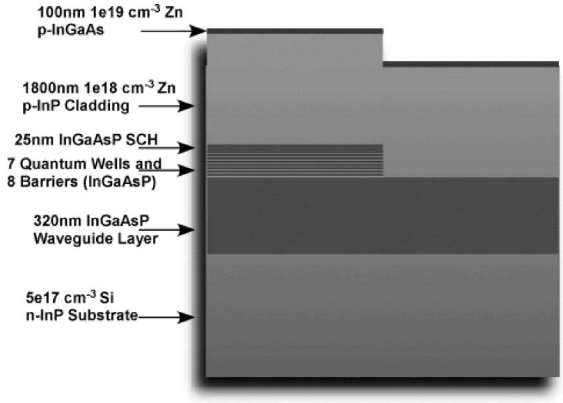

Fig. 4. Cross-sectional view of the active and passive region structure for offset quantum-well platforms.

arm is made slightly smaller, by reducing the input signal power in that arm, to match the phase state of the nondelayed arm.

The process described earlier causes the input data pulses to carve out pulses onto the CW signal, resulting in wavelength conversion. Both the rising and falling edges of the pulses are defined by the fast carrier depletion process. The device can also be made to operate in an inverting mode by setting the initial bias point of the MZI to an ON state and using the phase modulation to bring it into an OFF state. Since the cross-gain modulation works in favor of the output, the efficiency of the inverting scheme is higher, but it results in a dark pulse output that is not desirable for transmission.

B. Linear Input Preamplifiers

The input preamplifiers are required to amplify the input signal before wavelength conversion. It is crucial for these SOAs to provide linear signal gain, and hence, avoid distortion of the input signal due to pattern dependence. To maximize the performance and the efficiency of the device, it is desirable to get the maximum possible gain out of these SOAs. Since SOAs with a high confinement factor (Γ) have a low output saturation power and generate a much higher amount of amplified spontaneous emission (ASE), to achieve linear operation at high output powers, low confiment SOAs are required. In the devices presented in this paper, an offset quantum-well-based active region was used to fabricate these SOAs. Fig. 4 shows a cross-sectional view of the epitaxial layer structure for the offset quantum platform. The quantum wells in the active region are offset from the center of the waveguide, resulting in a low modal overlap, and hence, low confinement factor. In the design used in this paper, the active region overlap was 6%. Finally, based on measurements made on devices with different SOA lengths, a preamplifier length of 600 μm was used.

C. Nonlinear SOAs in the MZI

The most important components in the operation of the wavelength converters are the SOAs within the MZI structure. The nonlinear phase change in these amplifiers forms the basis of the wavelength conversion scheme [12]. The dynamic performance of the wavelength converters depends on the gain recovery

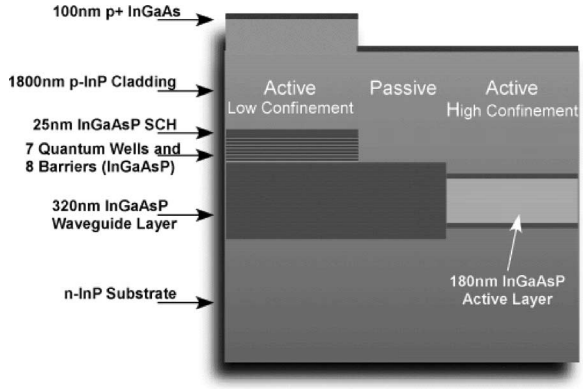

Fig. 5. Cross-sectional view of the active and passive region structure for hybrid offset quantum well and bulk-active platform.

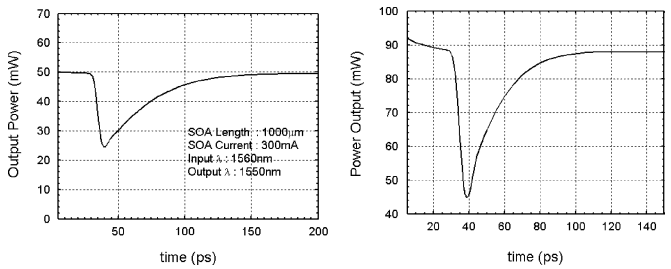

Fig. 6. Simulation of the gain recovery dynamics of OQW and bulk active region type SOAs. The SOA lengths were chosen to be 1 mm, the injection current was equal to 300 mA, the input wavelength was set at 1560 nm, and the output wavelength at 1550 nm.

time, and the amount of phase change in the MZI-SOAs. The gain recovery time determines the bandwidth of the wavelength converter, while the amount of phase change determines the power and the optical signal-to-noise ratio (OSNR) of the output signal [13]. A fast gain recovery time and large phase swing is crucial to achieving good performance at 40 Gb/s. An offset quantum-well-type active region, due to its low confinement, results in a slow gain recovery time and small phase swings. To improve the performance of the wavelength converters, a bulk-active region was used in the nonlinear SOA components in the second generation of devices. A butt-joint growth-based integration platform was used to achieve a hybrid offset quantum well and bulk-active structure, to incorporate a low confinement structure for the linear SOAs along with a high-confinement structure for the nonlinear MZI-SOAs. Fig. 6 shows a cross section of the different epitaxial regions in this platform. This platform allowed for independent optimization of the active regions in the two linear and nonlinear components on-chip. A simulation of the gain recovery dynamics in OQW and bulk active region type SOAs is shown in Fig. 6. The simulations indicate that the bulk-active region should be able to achieve significantly lower gain recovery times (40 ps) compared to an offset quantum-well active region (90 ps).

D. Choice of Proper Differential Delay

Monolithic integration of the DMZI devices requires the delay to be created on-chip, and it is therefore desirable to use as small a delay as possible to maximize the device integration density and minimize the optical propagation losses. To make the right design choice, the variation in the quality of the output signal as a function of the differential delay was determined [14]. An offset quantum-well-based SOA-MZI wavelength converter was used in these experiments. Fig. 7 shows a schematic of the devices used in this experiment. These devices were designed to have two input ports to allow signals to be independently coupled to the two MZI branches.

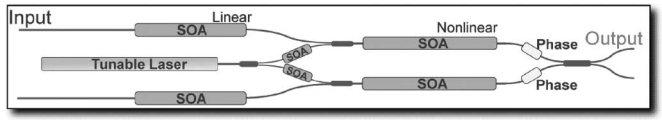

Fig. 7. Schematic diagram of the monolithic widely tunable wavelength converter used in the external differential delay experiments.

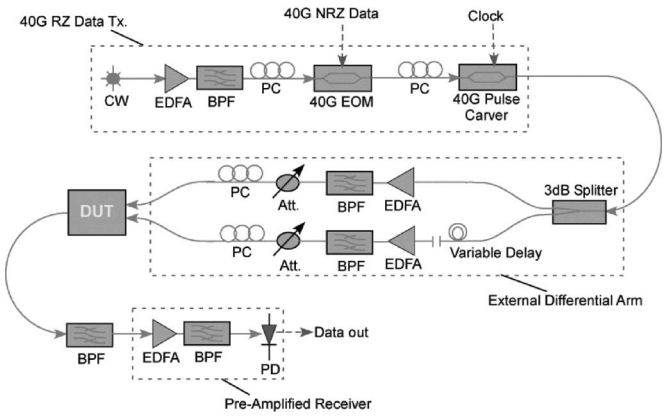

Fig. 8. Experimental setup used in the differential delay characterization of the widely tunable differential SOA-MZI wavelength converters.

The input signal used in these experiments had a full-width at half-maximum pulsewidth of 11 ps. The input signal was split into two paths, which were delayed with respect to each other; this delay was controlled using a free-space delay line in order to characterize the effect on the wavelength conversion. Angling the input waveguides of the device in the opposite directions allowed the two fibers to be independently coupled to the device on the same facet. The typical coupling loss for the setup was 4 dB. The output signal of the device was filtered using a 1.2-nm-wide filter to remove the input signal wavelength and then sent through a preamplified receiver to a 50-GHz photodetector. The preamplified receiver had a sensitivity of -32 dBm, which is typical for such receiver designs. The experiments were performed using PRBS $2^{31} - 1$ RZ data and the bit-error-rate (BER) measurements were performed on the received signal using an SHF 40-Gb/s BERT. The experimental setup is shown in Fig. 8.

The operating point of the wavelength converter was optimized by controlling the relative delay and the relative preamplifier gain of the two input arms. The differential delay was varied at the device input from 6.67 to 13.33 ps, and the BER measurements were performed. The signal quality was optimized for each delay by adjusting the relative input preamplifier gains and

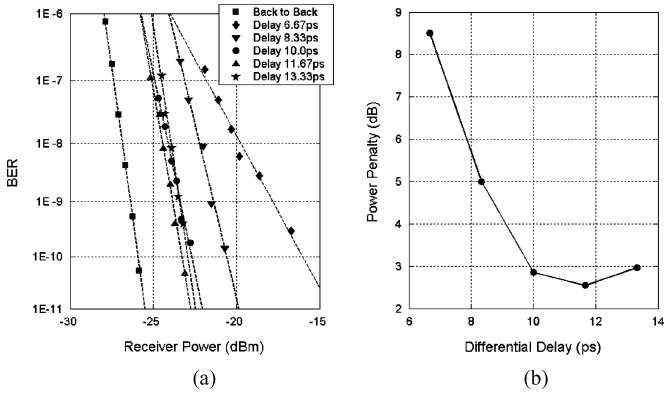

Fig. 9. BER measurements at different differential delay setting for a OQW-based SOA-MZI wavelength converter. (a) The BER curves obtained. (b) The measured power penalty at 10^{-9} error rate. The back-to-back was performed at 1543 nm.

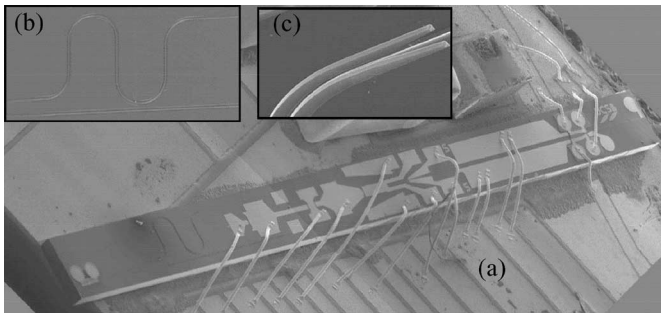

Fig. 10. (a) SEM image of a fabricated monolithic differential SOA-MZI wavelength converter. (b) SEM of the serpentine deep-etch waveguide used to achieve the differential delay. (c) A zoomed-in view of the surface to deep-etch ridge transition.

the MZI bias state, to achieve the best possible performance. The input wavelength was set at 1550 nm and the device was tuned to 1543 nm. Fig. 9(a) shows the BER curves obtained at different delay values. We see that as the delay is reduced below 10 ps, the BER curves tend to move away from the back-to-back, which signifies a degradation in signal quality. The variation in power penalty as a function of the differential delay can be seen in Fig. 9(b), which shows the power penalty obtained at different differential delays. It can be seen that a delay of around 11.5 ps is optimal. This required differential delay correlates very well with the input pulsewidth of 11 ps. A greater delay does not cause any degradation but, for monolithic integration, the smallest possible delay is required to minimize the chip area and the passive loss. Based on these measurements, and keeping in mind the requirement to keep the delay no larger than that required, the differential delay was chosen to be 10 ps.

III. Monolithic Tunable SOA-MZI Wavelength Converters—Performance

Fig. 10 shows an image of the monolithic wavelength converter of the first generation, incorporating the differential delay on-chip. A 10-ps differential delay, as determined in the previous section, requires the waveguides to have a length difference of 800 μm. In order to achieve such a length difference in a compact manner, a deeply etched ridge delay structure was used. The strongly confined waveguide allowed the use of bends with a small radius. This strongly guided waveguide structure was adiabatically coupled to a surface ridge structure used in the other components on-chip. The adiabatic taper utilizes linear tapering of the waveguide layer to achieve the transition between the surface ridge and the deep ridge. The fabrication of this section was performed using a two-step reactive ion etching process and the taper region was 40 μm long. We estimated the excess loss of the taper, based on beam propagation simulations, to be less than 0.2 dB for the misalignment tolerances expected in our etch process. The deeply etched waveguides that form the delay line utilized bends of 75-μm radius, and the overall loss of a 800-μm-long ridge was measured to be 3 dB. The inset shows an SEM of the serpentine pattern used to fabricate the delay. The resulting devices were 7 mm long and 0.5 mm wide. A schematic of the experimental setup used to measure the performance of the devices is shown in Fig. 11.

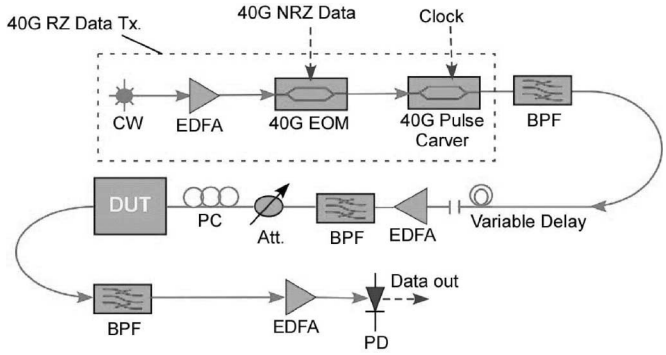

Fig. 11. Experimental setup used for the operation of the monolithic widely tunable differential SOA-MZI wavelength converters.

A. OQW-Based Devices

A OQW platform was used to prototype the monolithic wavelength converters, with compresively strained quantum wells that were 7 nm wide, and with 9-nm-wide tensile strained barriers. The waveguide used in all structures was 320-nm-thick 1.4Q InGaAsP. The surface ridge waveguides were 3 μm wide in device areas. The deep ridge waveguides were 2 μm wide. More details about the offset quantum-well epitaxial structure and process can be found in [6], [15], and [16]. The devices were operated at 40-Gb/s RZ data rates. The input data was generated using the transmitter illustrated in Fig. 11, and was modulated using a PRBS $2^{11}-1$ data sequence. For the measurements done on the fully integrated wavelength converter, PRBS $2^{11}-1$ sequence was used due to the limitation of the BER tester available to us. Due to a hardware issue in the tester, sequences longer than 2^{11} could not be generated with error-free performance at the time these measurements were performed. The signal traces in Fig. 12 do indeed show pattern dependence, but the effect tends to saturate after a few bits. One can see that there was no change in the power penalty between PRBS 2^7-1 and $2^{11}-1$ sequences, which leads us to expect that the device performance would not deteriorate further with longer data sequences. Fig. 12 shows an example of a wavelength-converted

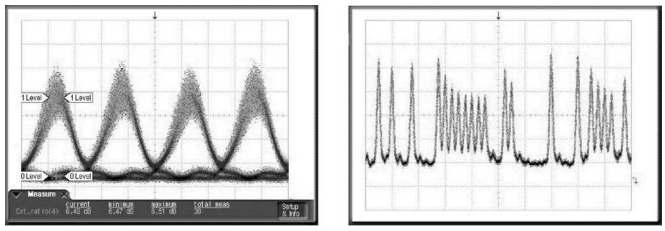

(a) (b)

Fig. 12. Wavelength-converted signal at the output of the OQW-type monolithic differential SOA-MZI wavelength converters. The input wavelength was set at 1553 nm and the output of the device was tuned to 1545 nm.

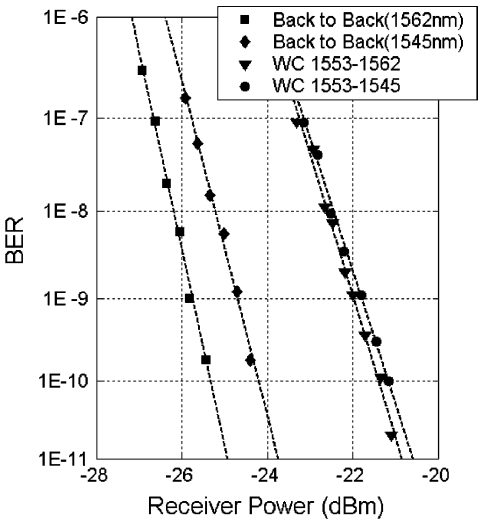

Fig. 13. BER measurements performed at 40 Gb/s on the OQW platform-based monolithic differential SOA-MZI wavelength converters.

output signal eye. Also shown in the figure is a trace of the pulse stream, which clearly shows the effect of the pattern dependence on the output signal. The OQW-based devices were able to achieve an extinction ratio of around 8 dB.

The BER measurements were performed on the wavelength-converted signal. The input wavelength was set at 1553 nm for these measurements and the output wavelength was tuned to 1545 and 1560 nm to gauge the performance of the devices for both up and down conversion. The results of the BER experiments are shown in Fig. 13. The input power level for the devices was 7 dBm and the output power in the fiber was around -10 dBm. The insertion loss at the input and the low conversion efficiency were primarily responsible for the low overall device efficiency obtained.

The wavelength-converted signal showed power penalties between 3 and 4 dB, which correlates very well with the results obtained using an external differential delay at 10 ps. Even though error-free wavelength conversion was obtained, the quality of the wavelength-converted signal in terms of its jitter, OSNR, and extinction ratio, is visibly degraded.

B. Bulk Active-Based Devices

A modified offset quantum-well platform, utilizing butt-joint growth (BJG) for MZI-SOA bulk-active region definition, was

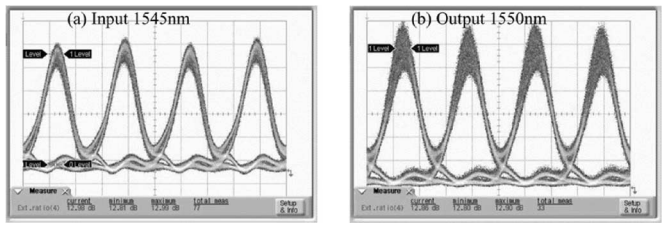

Fig. 14. Wavelength conversion result with the butt-joint growth platform-based differential SOA-MZI wavelength converters. (a) Input signal at 1545 nm. (b) Converted output at 1550 nm.

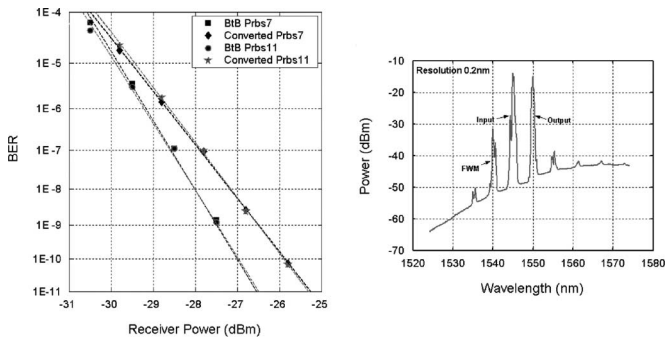

(a) (b)

Fig. 15. (a) BER measurement result for the BJG platform-based devices for PRBS $2^7 - 1$ and $2^{11} - 1$ data sequences. The input and output wavelengths were set at 1550 and 1545 nm, respectively. (b) The signal spectrum at the output of the devices.

used to fabricate devices with the same design specifications as the OQW devices. For these devices, we utilized the same quantum-well design as described previously. The bandgap of the bulk active layer was 1565 nm and the layer thickness was 180 nm, in order to best match the mode in from the 320-nm-thick 1.4Q InGaAsP waveguide layer. These devices achieved a majorly improved performance compared to the OQW devices due to greater cross-phase efficiency of the wavelength conversion and faster gain recovery times in the bulk MZI-SOAs. The output extinction ratio is close to 13 dB, which was as good as that of the input signal. The wavelength-converted output for a set of input and output wavelengths is shown in Fig. 14. The BER measurements were performed using both PRBS $2^7 - 1$ and $2^{11} - 1$ data stream, to measure any degradation that long pattern lengths would introduce into the signal. The BER results for the two data streams are shown in Fig. 15(a). The input and output eye diagrams for these measurements are shown in Fig. 14. The results for the two pattern lengths are nearly identical, which shows that longer pattern lengths do not introduce any additional penalty into the system. Also shown in Fig. 15(b) is a spectrum analyzer trace of the wavelength-converter output. The input, output signals and the four-wave mixing (FWM) tone are clearly visible. The input power level for the devices was 10 dBm, and the output power levels were around -8 dBm. The reason for the excessive input power requirement was the passive loss in the input waveguide due to a fabrication error. Fabrication process modifications have been determined to prevent this from occurring in future device generations. The

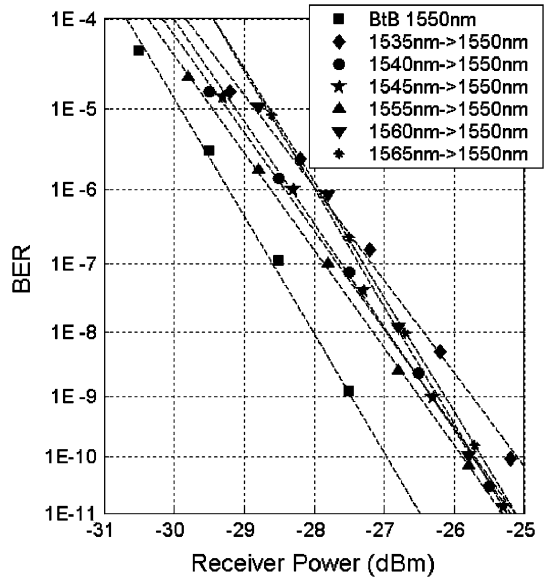

Fig. 16. BER measurements for the BJG-based devices for a fixed output wavelength and a varying input wavelength. The output wavelength is fixed at 1550 nm.

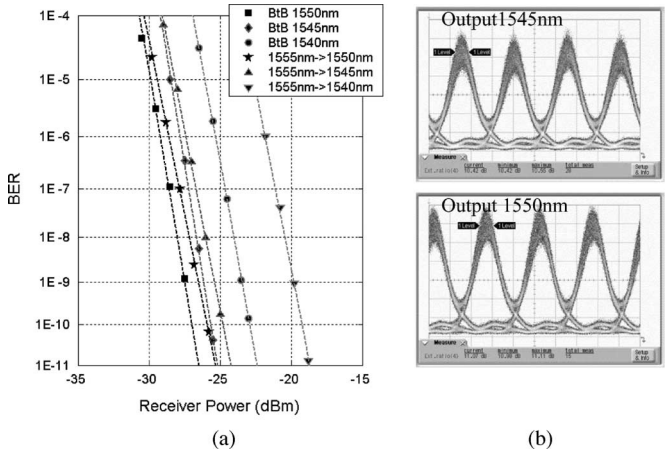

Fig. 17. (a) BER measurement results for a fixed input and varying output wavelength. (b) Example of the wavelength-converted eyes for certain output wavelengths.

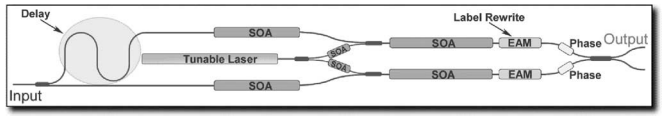

Fig. 18. Schematic diagram of the monolithic PFC showing the various functional elements.

wavelength sensitivity of these designs was also studied. The first set of measurements were performed keeping the output wavelength of the device fixed while the input signal wavelength was scanned. Fig. 16 shows the results obtained from these experiments. The output wavelength was fixed at 1550 nm and the input wavelength was scanned across the C-band from 1535 to 1565 nm. The measured power penalty varied from 0.7 dB for input wavelengths close to the gain peak to around 1.5 dB for wavelength further away from the gain peak, which was a big improvement compared to the penalty obtained using the OQW devices. The improved performance of the wavelength converter was achieved by using the bulk-active region in the MZI-SOAs, which allowed for greater cross-phase modulation efficiency of these devices compared to that of the low-confinement OQW design. Finally, measurements were performed keeping the input wavelength to the device fixed and varying the output wavelength of the device. As the SGDBR's lasing wavelength moves away from the gain peak of the quantum wells, the decrease in differential efficiency increases the carrier recovery lifetime in the SOAs, leading to a degradation in performance. The BER results for different output wavelength are shown in Fig. 17. The gain peak for the bulk active material used in these device was centered close to 1560 nm, and therefore, output wavelengths of 1550 and 1545 nm show good results with a less than 1-dB power penalty. However, the power penalty increases to around 3 dB for output wavelengths further away from the gain peak. The tuning range of the on-chip SGDBR laser prevented the testing of these devices for output wavelengths longer than 1555 nm.

IV. Monolithic PFC in InP

In addition to steering packets based on wavelength, an optical packet switch must also have the capability to erase and rewrite the new optical labels while the payload is switched. The combined process of wavelength switching and attaching new header information on the outgoing packet is known as packet forwarding. In this section, we present results related to the operation of our monolithic InP-based PFC, which incorporates three main routing functions needed for packet-switched networks: fast wavelength switching, wavelength conversion, and electro-optic label encoding. The devices that we used to achieve these functions, incorporate a 40-Gb/s all-optical differential wavelength converter, a fast tunable laser, and a 10-Gb/s electrical modulator on a single chip.

A. Design of the PFC

A novel feature of this device is that a bulk Franz–Keldysh modulator was designed to be a part of the MZI to allow electrical switching of the MZI, along with the optical switching allowed by the SOAs. The modulator is implemented using the same passive waveguide structure like the phase electrodes, or MMI splitters, with an additional step of removing about 100 nm of the top waveguide layer, in order to remove the P-doped section of the waveguide around the modulator and to reduce the modulator capacitance. More details about the modulator design in this platform can be found in [17].

A schematic of the monolithic PFC is shown in Fig. 18. The SGDBR laser was used as an on-chip (fast-tunable at the packet rate) light source, and designed to provide full C-band coverage. A 10-ps differential delay, fabricated using a deeply etched waveguide, was used in the wavelength converters. The preamplifiers SOAs were 600 μm long and the MZI-SOAs were designed to be 1.2 mm in length.

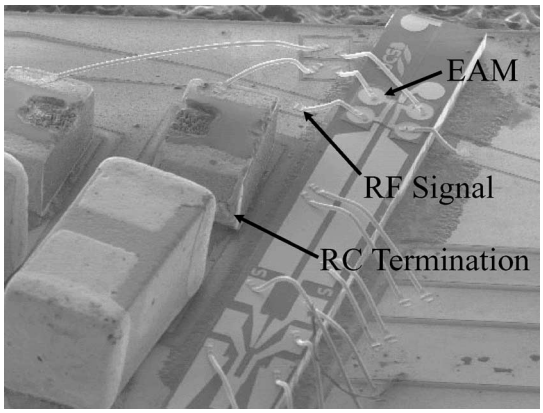

Fig. 19. Image of the EAM section of the PFC mounted on carrier showing the wire-bond arrangement.

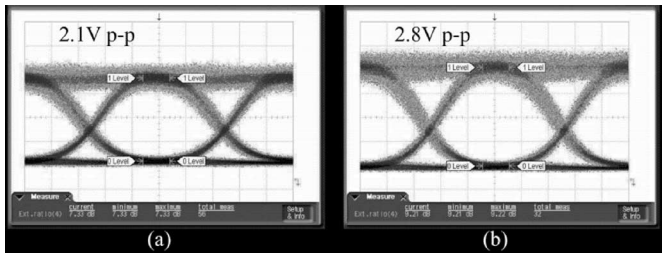

Fig. 20. Eye diagrams of the electrically modulated signal from the packet-forwarding devices at 10 Gb/s-NRZ data rates for voltage swings. (a) 2.1 V. (b) 2.8 V.

The bulk Franz–Keldysh-type electro-absorption modulator (EAM) sections in the MZI were chosen to be 250 μm long. This length was expected to provide the neccessary amount of phase swing while keeping the capacitance and insertion losses low, allowing efficient 10-Gb/s operation. The signals from the two MZI arms are combined at the device output using a 2×2 MMI coupler. The fabricated chips were 7 mm long and 0.5 mm wide. The results presented in the following sections are for the PFCs fabricated in the offset quantum-well platform.

B. Performance of the PFC

1) Electrical Modulation At 10 Gb/s: Modulation characteristics of the EAMs were measured at 10-Gb/s data rate. The label encoding is in the nonreturn-to-zero (NRZ) format. The devices were mounted on an aluminum nitride (AlN) carrier, and a coplanar line was traced on the carrier to create the high-speed electrical connection with the EAM section. The EAM was then RC terminated to the ground using a 50-Ω resistor. Fig. 19 shows an image of the EAM section of a mounted and wire-bonded device.

Modulator experiments were performed using 10-Gb/s PRBS data. Since the EAM sections were intended for use with short headers that did not contain long pattern lengths, a PRBS $2^7 - 1$ sequence was used. The electrical signal was generated using an Anritsu BERT, and amplified using an SHF 12-GHz amplifier, which provided 17 dB of gain. A bias-tee was used to set the dc level of the electrical signal and the signal was then coupled to the EAM using a coplanar waveguide (CPW) probe. The SGDBR laser was turned on, and the MZI-SOAs were biased at 250 mA each. The phase electrode in the MZI was adjusted to achieve the maximum extinction ratio on the output optical signal. The signal was then sent to a preamplified receiver through an attenuator, which was used to control the receiver input power during BER testing.

The dc bias level for the EAM, set using the bias-tee arrangement, determines its operating point on the transfer function. The amount of phase swing generated by the modulators is then determined by the RF peak-to-peak amplitude applied to the device. Electrical modulation of the PFC was performed at varying RF voltage levels to determine the voltage swing required to achieve good output extinction ratio. Fig. 20 shows the modulator output from the device at RF voltage amplitudes of 2.1 and 2.8 V. As expected, higher RF voltages produced greater voltage swings and led to a greater extinction ratio for the output signal.

Packet traffic, however, is bursty in nature, consisting of short bursts of data followed by long durations of zero signal. This bursty nature is further pronounced in the case of packet header data that forms a small fraction of the packet itself. This poses strong challenges for the electronic and photonic components designed to handle such traffic. The packet format used in the experiment presented here required a 128-b header (12.8-ns duration). This was short enough that even though the thermal chirp caused significant distortion of the modulated signal, it could still be detected error-free. To measure the error performance of header modulation, the header signal was generated using a pattern generator. Variable-length packet data traffic was simulated in the experiment. The pattern generator used a 60-packet-wide data stream to mimic variable-length packet traffic conditions. Each 60-packet frame of the data stream contained a 7:4:1 packet payload size ratio, i.e., 7×40 byte payloads (8 ns), 4×570 byte payloads (114 ns), and 1×1500 byte long payloads (300 ns). A header was generated for each payload, and padded with zeros in between. This packet stream, which we labeled Imix stream since it mimics the Internet traffic conditions, was also used to generate the 40-Gb/s payloads. The BER measurements performed on the headers of the actual Imix packet data are shown in Fig. 21. The BER curves follow the same trend for varying voltage swings as the PRBS measurements. However, the improvement in sensitivity with voltage swing tends to saturate toward the high voltages due to the increased distortion introduced by the thermal effects. The BER measurements performed on the header data show a much lower sensitivity that the PRBS measurements due to the much lower duty cycle of the Imix data stream. A factor of approximately 12 dB is required to adjust for the difference in duty cycle between the two data streams.

2) Optical Wavelength Conversion at 40 Gb/s: As explained in the previous section, for all practical purposes and applications, it is important to gauge the performance of the PFC in the packet mode. Measurements were done using 40-Gb/s payloads to verify that packet format data did not introduce any additional signal distortions. The 40-Gb/s PRBS signal generated by the

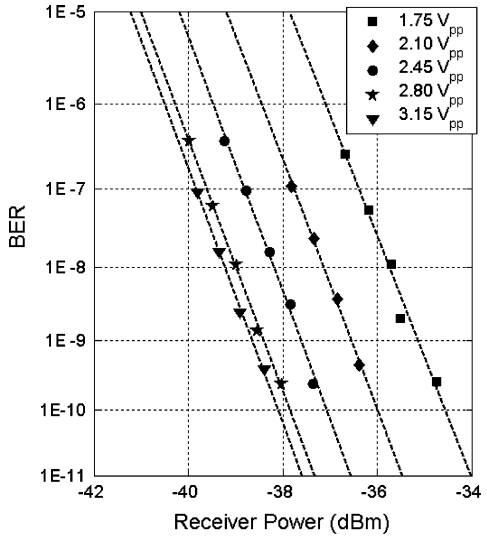

Fig. 21. BER measurements for varying voltage swings for an Imix header stream at 10 Gb/s-NRZ data rate.

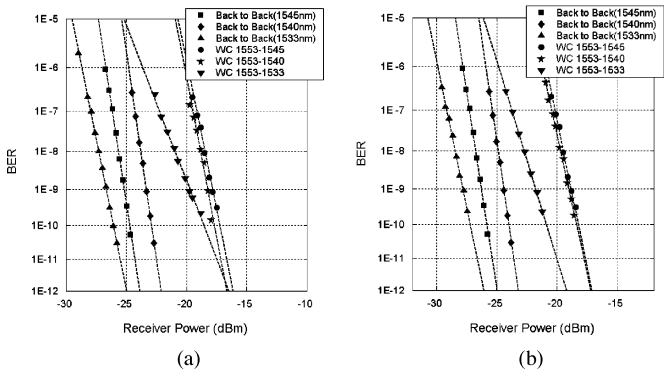

Fig. 22. BER measurement results for 40-Gb/s wavelength conversion. (a) PRBS. (b) Packet data for varying output wavelengths.

data transmitter was carved into packets using a lithium niobate modulator. The data was gated to generate 300-ns-long packets with 100-ns guard bands. The packet carving signal was generated using an arbitrary waveform generator (ARB), which also generated the gating signal for the BERT. The PFC was operated under the same conditions as those for PRBS data and the BER performance of the converted payload was measured on the SHF 40-Gb/s BERT. The BER measurements for PRBS and packet data on an OQW-based PFC chip are shown in Fig. 22 for a varying set of output wavelengths. The device used in these experiments resulted in a slightly higher power penalty, compared to the results shown in the previous sections of this paper. However, the important result in these measurements was that no additional power penalty was observed for operating the devices with packet format data. The devices were also used to demonstrate packet forwarding using an optical packet switch testbed and layer-2 measurements. These experimental results are detailed in [18] and [19].

V. Conclusion

The objective of this paper was to present the advanced wavelength converter technologies developed in InP for high-speed packet-switched optical networks. We have demonstrated monolithic widely tunable all-optical differential SOA-MZI wavelength converters operating at 40 Gb/s. The devices incorporated the required differential delay on-chip to realize single-input–single-output wavelength converters operating at 40 Gb/s. The PICs required various different active and passive components, meeting different performance requirements on a single chip. A butt-joint growth-based integration platform was explored to incorporate both high- and low-confinement active regions in the same device.

It was found that the wavelength converters fabricated in the butt-joint growth platform, which allowed for the fabrication of two independent active material layer stacks, achieved best performance. Low-confinement SOAs fabricated using the offset quantum-well stack provided high output saturation powers and were well suited for use as linear preamplifiers, while high confinement bulk-active regions in the MZI proved to be very efficient as nonlinear elements. The devices showed excellent performance at 40-Gb/s data rates. Very low jitter and output extinction ratios in excess of 12 dB were obtained and BER measurements showed a conversion penalty of less than 1 dB across the C-band.

The device functionality was extended by incorporating an electrical modulation stage into the devices to realize a monolithic PFC. These devices realized three major functions required for a high data rate packet-switched network in a single monolithic device, allowing for simultaneous tunability, all-optical wavelength conversion, and optical label encoding. The device monolithically integrated a fast switchable widely tunable SGDBR laser, a 40-Gb/s RZ differential SOA-MZI wavelength converter, and a 10-Gb/s label encoder. The label encoder was designed using a bulk Franz–Keldysh electro-absorption modulator as part of the MZI. This scheme allowed both electrical and optical control of the MZI to achieve label rewrite and wavelength conversion simultaneously. The devices were tested using packet data, and the BER measurements were performed to verify independent and simultaneous error-free operation of packet conversion and label rewrite.

References

[1] K. G. Coffman and A. M. Odlyzko. (Oct. 1998). The size and growth rate of the Internet, *First Monday* [Online]. Available: http://firstmonday.org/ (also available: http://www.research.att.com/˜amo).

[2] —— "Internet growth: Is there a "Moore's law" for data traffic?," in *Handbook of Massive Data Sets* Norwell, MA: Kluwer, 2001.

[3] D. Blumenthal, B. E. Olsson, G. Rossi, T. E. Dimmick, L. Rau, M. Masanovic, O. Lavrova, R. Doshi, O. Jerphagnon, J. E. Bowers, V. Kaman, L. A. Coldren, and J. Barton, "All-optical label swapping networks and technologies," *J. Lightw. Technol.*, vol. 18, no. 12, pp. 2058–2075, Dec. 2000.

[4] S. Yao, S. J. B. Yoo, B. Mukherjee, and S. Dixit, "All-optical packet switching for metropolitan area networks: Opportunities and challenges," *IEEE Commun. Mag.*, vol. 39, no. 3, pp. 142–148, Mar. 2001.

[5] S. Yao, S. Dixit, and B. Mukherjee, "Advances in photonic packet switching: An overview," *IEEE Commun. Mag.*, vol. 38, no. 2, pp. 84–94, Feb. 2000.

[6] M. L. Mašanović, V. Lal, J. Barton, E. Skogen, L. A. Coldren, and D. J. Blumenthal, "Monolithically integrated Mach–Zehnder interferometer wavelength converter and widely tunable laser in InP," *IEEE Photon. Technol. Lett.*, vol. 15, no. 8, pp. 1117–1119, Aug. 2003.

[7] T. Durhuus, C. Joergensen, B. Mikkelson, R. J. S. Pedersen, and K. E. Stubkjaer, "All-optical wavelength conversion by SOA's in Mach–Zehnder configuration," *IEEE Photon. Technol. Lett.*, vol. 6, no. 1, pp. 53–55, Jan. 1994.

[8] T. Durhuus, B. Mikkelson, C. Joergensen, S. L. Danielsen, and K. E. Stubkjaer, "All-optical wavelength conversion by semiconductor optical amplifiers," *J. Lightw. Technol.*, vol. 14, no. 6, pp. 942–954, Jun. 1996.

[9] J. Leuthold, J. Eckner, P. A. BEsse, G. Guekos, and H. Melchior, "Dual-order mode (DOMO) all-optical space switch for bi-directional operation," in *Proc. OFC'96 ThQ1, Opt. Fiber Commun. Conf.*, San Jose, CA, 1996, pp. 271–272.

[10] J. Leuthold, C. H. Joyner, B. Mikkelsen, G. Raybon, J. L. Pleumeekers, B. I. Miller, K. Dreyer, and C. A. Burrus, "100-Gbit/s all-optical wavelength conversion with integrated SOA delayed interference configuration," *Electron. Lett.*, vol. 36, no. 12, pp. 1129–1130, 2000.

[11] D. Wolfson, A. Kloch, T. Fjelde, C. Janz, B. Dagens, and M. Renaud, "40-Gb/s all-optical wavelength conversion, regeneration, and demultiplexing in an SOA-based all-active Mach–Zehnder interferometer," *IEEE Photon. Technol. Lett.*, vol. 12, no. 3, pp. 332–334, Mar. 2000.

[12] D. D. Marcenac, A. E. Kelly, D. Nesset, and D. A. O. Davies, "Bandwidth enhancement of wavelength conversion via cross-gain modulation by semiconductor optical amplifier cascade," *Electron. Lett.*, vol. 31, pp. 1442–1443, 1995.

[13] M. L. Mašanović, V. Lal, E. Skogen, J. Barton, J. Summers, J. W. Raring, L. A. Coldren, and D. J. Blumenthal, "Cross-phase modulation efficiency in offset quantum well and centered quantum well semiconductor optical amplifiers," *IEEE Photon. Technol. Lett.*, vol. 17, no. 11, pp. 2364–2366, Nov. 2005.

[14] V. Lal, M. L. Mašanović, J. A. Summers, L. A. Coldren, and D. J. Blumenthal, "Performance optimization of an InP-based widely tunable all-optical wavelength converter operating at 40 Gbps," *IEEE Photon. Technol. Lett.*, vol. 14, no. 4, pp. 183–186, Feb. 15, 2006.

[15] M. L. Mašanović, V. Lal, J. A. Summers, J. S. Barton, E. Skogen, L. G. Rau, L. A. Coldren, and D. J. Blumenthal, "Widely tunable monolithically integrated all-optical wavelength converters in InP," *J. Lightw. Technol.*, vol. 23, no. 3, pp. 1350–1362, Mar. 2005.

[16] M. L. Mašanović, "Wavelength agile photonic integrated circuits for all-optical wavelength conversion" Ph.D. dissertation, Univ. California, Santa Barbara, CA, Jun. 2004.

[17] J. S. Barton, E. J. Skogen, M. L. Masanovic, S. P. Denbaars, and L. A. Coldren, "A widely tunable high-speed transmitter using an integrated SGDBR laser-semiconductor optical amplifier and Mach–Zehnder modulator," *IEEE J. Sel. Topics Quantum Electron.*, vol. 9, no. 5, pp. 1113–1117, Sep.–Oct. 2003.

[18] V. Lal, M. L. Mašanović, D. Wolfson, G. Fish, C. Coldren, and D. J. Blumenthal, "Monolithic widely tunable optical packet forwarding chip in InP for all-optical label switching with 40 Gbps payloads and 10 Gbps lablels," presented at ECOC'05, Eur. Conf. Opt. Commun., Glasgow, Scotland, 2005.

[19] D. Wolfson, V. Lal, M. Masanovic, H. N. Poulsen, C. Coldren, G. Epps, D. Civello, P. Donner, and D. J. Blumenthal, "All-optical asynchronous variable-length optically labelled 40 Gbps packet switch," presented at the ECOC'05, Eur. Conf. Opt. Commun., Glasgow, Scotland, 2005.

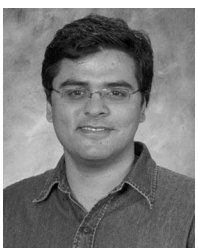

Vikrant Lal (M'04–M'06) received the B.S. degree in electrical engineering from the Indian Institute of Technology Delhi, New Delhi, India, the Master's degree in communications engineering from the Electrical and Computer Engineering Department, University of Maryland, College Park, and the Ph.D. degree in electrical and computer engineering from the University of California at Santa Barbara, Santa Barbara, in 1999, 2001, and 2006, respectively.

He is currently a Technical Staff Member with Infinera Corporation, Sunnyvale, CA. His current research interests include photonic integrated circuits, optical networking, and all-optical switching.

Milan L. Mašanović (S'98–M'04) received the Dipl. Ing. degree from the School of Electrical Engineering, University of Belgrade, Belgrade, Yugoslavia, and the M.S. and Ph.D. degrees from the University of California at Santa Barbara, Santa Barbara, in 1998, 2000, and 2004, respectively, all in electrical engineering.

He is currently a Research Scientist at the University of California at Santa Barbara. He is also a founder of Freedom Photonics, a photonic integration company in Goleta, CA. He is the author or coauthor of more than 70 research papers. His current research interests include InP photonic integration related to applications in packet-switched optical networks.

Dr. Mašanović was the recipient of the 2004 IEEE Lasers & Electro-Optics Society Graduate Student Fellowship Award and the 2003 Best Student Paper Award at the Indium Phosphide and Related Materials Conference.

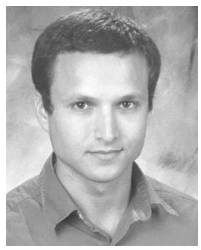

Joseph A. Summers (S'04–M'06) received the B.S. degree in electrical engineering from Northwestern University, Chicago, IL, in 2000. He is currently working toward the Ph.D. degree in electrical and computer engineering at the University of California at Santa Barbara, Santa Barbara.

His current research interests include high-density photonic integrated circuits and academic outreach.

Greg Fish, photograph and biography not available at the time of publication.

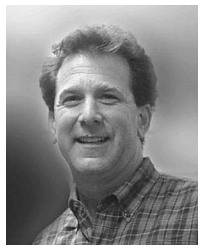

Daniel J. Blumenthal (S'91–M'93–SM'97–F'03) received the B.S.E.E. degree from the University of Rochester, Rochester, NY, the M.S.E.E. degree from Columbia University, New York, and the Ph.D. degree from the University of Colorado, Boulder, in 1981, 1988, and 1993, respectively, all in electrical engineering.

In 1981, he was with StorageTek, Louisville, CO, and during 1993–1997 he was an Assistant Professor at the School of Electrical and Computer Engineering, Georgia Institute of Technology, Atlanta. He is currently a Professor in the Department of Electrical and Computer Engineering, University of California at Santa Barbara (UCSB), Santa Barbara. He is the Director of the LASOR Center at UCSB, a project funded by the Defense Advanced Research Projects Agency Data in the Optical Domain Network (DOD-N) Program and currently serves on the Board of Directors for National LambdaRail. He is also the Cofounder of Calient Networks, an optical switching system company. He is the author or coauthor of over 230 research papers and is the coauthor of *Tunable Laser Diodes and Related Optical Sources* (New York: IEEE-Wiley, 2005). His current research interests include optical communications, photonic packet-switched and all-optical networks, all-optical wavelength conversion, ultra-fast communications systems, integrated photonic circuits, and nanophotonic technologies.

Dr. Blumenthal was the recipient of the 1999 Presidential Early Career Award for Scientists and Engineers from the White House, the 1994 National Science Foundation Young Investigator Award, and the 1997 Office of Naval Research Young Investigator Program Award. He has served as an Associate Editor for IEEE PHOTONICS TECHNOLOGY LETTERS and IEEE TRANSACTIONS ON COMMUNICATIONS, as a Guest Editor for the IEEE JOURNAL OF LIGHTWAVE TECHNOLOGY special issue on photonic packet switching systems and the IEEE JOURNAL OF SELECTED AREAS IN COMMUNICATIONS special issue on high-performance optical/electronic switches/routers for high-speed Internet. He has served as the General Program Chair for the 2001 Optical Society of America (OSA) Topical Meeting on Photonics in Switching and as Program Chair for the 1999 Meeting on Photonics in Switching. He has also served on numerous other technical program committees. He is a Fellow of the OSA.